Supporting Information for:

TPD of Nitric Acid on BaNa-Y: Evidence that a Nanoscale Environment Can Alter a Reaction Mechanism.

Aditya Savara, Alon Danon, Wolfgang M.H. Sachtler, and Eric Weitz*

Department of Chemistry and the Institute for Catalysis in Energy Processes, Northwestern University, 2145 Sheridan Road, Evanston, IL 60208

I. TPD Analysis of Surface Nitrate Depletion

As shown below, the depletion of surface nitrates during TPD can be described by either a second-order desorption process where all sites have a common activation energy, or a first-order process with a distribution of activation energies (site heterogeneity). These two cases cannot be distinguished between without further experiments. The kinetics for depletion of an adsorbate are described using the equation:[1]

$$-\frac{d\theta}{dT}\left(\frac{1}{\theta^{n}}\right)=\frac{k_{0}}{\beta_{H}}\exp\left(\frac{-E_{A}}{RT}\right) \qquad (S.1)$$

where θ is the fraction of surface sites covered by the adsorbate for a given type of surface site, β_H is the heating rate, k_0 is the pre-exponential for desorption, ***n*** is the order of the desorption process, E_A is the activation energy for desorption (from this type of site), and the other variables have their usual meaning. A desorption, with ***n***=2, is often characteristic of a rate limiting second-order recombination of surface species prior to desorption. The units for k_0 are s^{-1} regardless of the order of desorption, ***n***, since in Eq.

S.1 the adsorbate surface concentration is expressed as a unitless relative site coverage, θ.[2]

Depending on the mechanism, the depletion of surface nitrates could be either first-order or second-order. If the surface NO_3^- depletion occurs without the participation of H^+, a first-order process is expected. If the depletion of NO_3^- takes place due to recombination of NO_3^- and H^+ followed by desorption, e.g.

$$H^+ + NO_3^- \rightarrow \text{intermediate} \rightarrow HNO_3(g),$$

the order of reaction could be either first-order or second-order, depending on whether the highest free energy barrier in the reaction mechanism is before or after recombination.

To find the order and kinetic parameters for nitrate depletion, Eq. S.1 was fit to the TPD data for nitrate depletion with both $\boldsymbol{n} = 1$ and $\boldsymbol{n} = 2$. Fitting with Eq S.1 with n=2 yields $k_o = 1.86 \times 10^{15} \pm 1.16 \times 10^{15}$ s^{-1} and $E_A = 212 \pm 5$ kJ mol^{-1} -- adequately describing the curve (R^2=0.9932) with physically realistic parameters.[2] In contrast, fitting with Eq. S.1 with n=1 yields a fit ($R^2 = 0.9762$) with physically unrealistic[2] values for k_0 and E_A ($k_0 = 1.17 \times 10^3 \pm 0.61 \times 10^3$ s^{-1} and $E_A = 69 \pm 3$ kJ mol^{-1}). Constraining the first-order fit to have a more realistic[2] k_0 of $\geq \sim 10^9$ leads to $k_0 = 0.96 \times 10^9 \pm 0.32 \times 10^9$ s^{-1} and $E_A = 144 \pm 18$ kJ mol^{-1} with a poor R^2 of 0.7795. However, the poor R^2 for the first-order (n=1) constrained fit could be a result of multiple sites with different activation energies for desorption, which would lead to deviations in the behavior of the TPD curve relative to what is predicted by Eq. S.1.[1]

Figure S.1 shows that while a single first-order TPD peak cannot produce the shape of the experimentally observed TPD peak, a set of sites with different activation energies undergoing first-order desorption can. The dashed curves represent simulated

first-order TPD peaks with $k_0=10^{13}$ and desorption activation energies, E_A of 160 kJ mol^{-1}, 173kJ mol^{-1} and 186 kJ mol^{-1} with sites that have fractional contributions to the total coverage of 0.2, 0.3, and 0.5 respectively. These parameters were chosen based on trial and error to find realistic parameters which semi-quantitatively reproduce the experimental curve. Programs that are used to deconvolute complex overlapping TPD peaks often assume a Gaussian function or similar function for the distribution of energies of the individual peaks, which center around several discrete energies (such as 160 kJ mol^{-1}, 173kJ mol^{-1} and 186 kJ mol^{-1}).[3] This simulation indicates that a distribution of sites that have activation energies ranging from ~160 to 190 kJ mol^{-1} where each site undergoes a first-order desorption process could result in the experimentally observed TPD data.

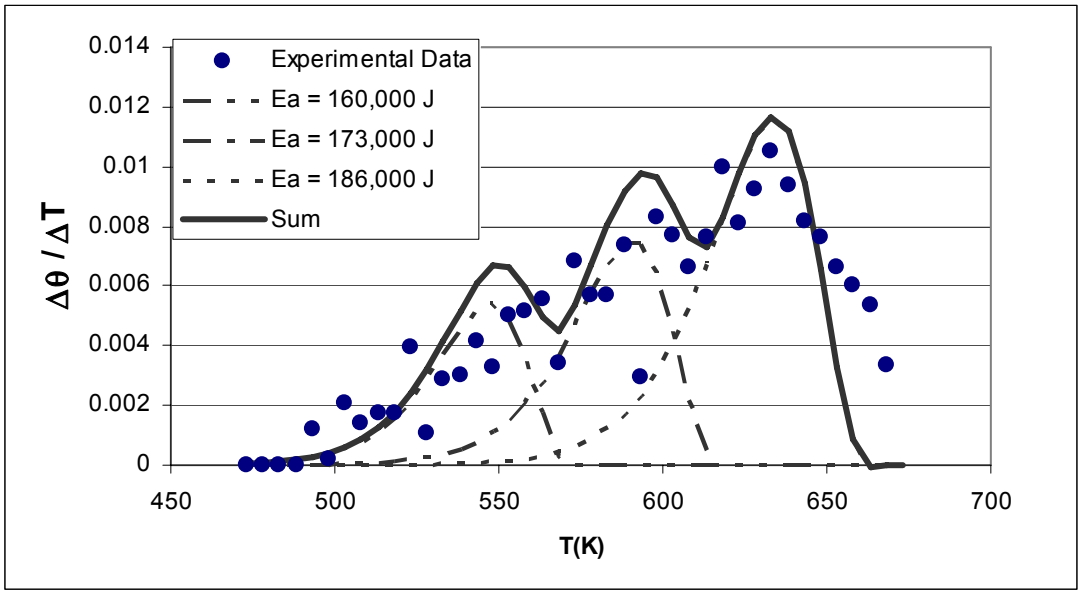

Figure S.1: Experimental TPD data with simulated first-order TPD signals arising from a distribution of sites with $k_0=10^{13}$. Individual simulated site contributions are shown with dashed lines, with the total simulated signal shown in a thick solid line.

Further treatment of the TPD data is possible using Redhead's analysis:[1]

$$\frac{E_A}{RT_P} = \ln\left(\frac{k_o T_P n \theta_P^{n-1}}{\beta_H}\right) - \ln\left(\frac{E_A}{RT_P}\right) \quad \text{(S.2)}$$

T_P is the temperature of the maximum rate of desorption (the maximum of dθ/dT vs. T), $\boldsymbol{n}$ is the order of the desorption process and θ_P is a constant which drops out for a first-order desorption process, while $\theta_P = \theta_0 / 2$ for a 2nd order desorption process (θ_0 is the initial coverage during TPD). The observed T_P was always between 350 and 375 °C, a range which corresponds well with results reported by Szanyi et al. in similar experiments.[4] Predicted ranges for T_p were obtained for the first and second-order models, using Eq. S.2 and the fitted parameters for E_A and k_0 (from Eq S.1) with propagation of fitting error. Neither a first-order nor second-order process could be ruled out on the basis of this method, as both yielded temperature ranges that overlapped with the observed T_P. It has also been found empirically that for TPD experiments which have initial coverages near saturation, E_A/RT_P from Eq. S.2 is typically within 20% of the unitless value of 30.[1] This empirical correlation was also met for all of the models described above, except for the unconstrained first-order fit, which has already been ruled out as a plausible scenario.

From the above analysis, we conclude that we cannot determine whether the depletion of the surface nitrates involves a first-order or second-order rate limiting step without further experiments (e.g., varying initial coverage), which are beyond the scope of the main article. If desorption is rate limited by a second-order recombination, the rate equation is: rate = $k(\theta_{NO3}\text{-})(\theta_{H+}) = k(\theta_{NO3}\text{-})^2$, given that $\theta_{NO3}\text{-} = \theta_{H+}$ at all times. There are two plausible mechanisms for the depletion observed: H^+ and NO_3^- might directly react to

form intermediates or the products observed, or H^+ and NO_3^- might first combine to produce HNO_3 which then desorbs and decomposes. Both of these mechanisms, which can lead to formation of OH + NO_2, may be either first or second-order. The effective order is determined by whether recombination/reaction (2nd order) or desorption/decomposition (1st order) of the intermediate(s) is rate limiting,.

II. Rate of HNO_3 Gas Phase Decomposition vs. BaNa-Y TPD Nitrate Depletion

To check whether HNO_3 gas is a plausible intermediate in the TPD of H^+ and NO_3^- chemisorbed on BaNa-Y, the experimentally obtained rate of nitrate depletion was compared to the rate for decomposition of gas phase nitric acid calculated from accepted rate constants. As described in the main article, the rate of decomposition of gas phase nitric acid must be faster than the observed rate of surface nitrate depletion if gas phase nitric acid is an intermediate. The quantity of nitric acid which would be produced from the depletion of surface nitrates is calculated using the normalization of moles of NO_3^- as obtained via the procedure described in section IV.A.2 of the main article. The inequality in Eq S.3 must hold if the rate of gas phase decomposition for the nitric acid is faster than the depletion of surface nitrates:

$$\frac{-\Delta NO_3^-(ads)}{\Delta t} < \frac{-\Delta HNO_3(g)_{calc}}{\Delta t}. \qquad (S.3)$$

ΔNO_3^- is the moles of experimentally observed nitrate depletion during a given time-step (Δt) of 1 min during TPD . $\Delta HNO_3(g)_{calc}$ is the moles of nitric acid gas which would be be depleted due to gas phase nitric acid decomposition during the same time-step. For calculation of $\Delta HNO_3(g)_{calc}$, the time-step is assumed to be isothermal, and the initial quantity of HNO_3(g) at each time-step is assumed to be given by the surface nitrate depletion ($-\Delta NO_3^-$) from the same time-step. With these assumptions, $\Delta HNO_3(g)_{calc}$ is

the difference between the final and initial concentrations of HNO_3*(g)* during a given time-step, which is derived from the integrated rate law of a first-order reaction as:

$$\frac{\Delta HNO_3(g)_{calc}}{\Delta t} = \frac{[HNO_3(g)]_i - [HNO_3(g)]_f}{\Delta t} = \frac{[HNO_3(g)]_i(1 - e^{-k\Delta t})}{\Delta t} \qquad (S.4)$$

k is the literature value for Rxn 1-0 in Table S.2, which is dependent on temperature and is different for each time-step due to the increase of 5 °C per time-step in the TPD experiment. $[HNO_3(g)]_i$ is the quantity of HNO_3 at the beginning of a time-step (given by $-\Delta NO_3^-$ from the same time-step) and $[HNO_3\ (g)]_f$ is the quantity of $HNO_3(g)$ at the end of a time-step. As mentioned in the main article, the gas phase decomposition of HNO_3 follows a Lindemann mechanism. The experimentally observed rate for nitrate depletion is compared with the rate calculated for the unimolecular decomposition of nitric acid in Figure S.2, for several total pressures of "M". For [M]=1 Torr and [M] = 10 Torr, the calculated rate is lower than the TPD curve, indicating that the rate of gas phase nitric acid decomposition is too slow to be consistent with desorption followed by decomposition. For [M]=100 Torr and for the high pressure limit, the traces overlap with the TPD curve, indicating that at pressures ≥ 100 Torr the rate of gas phase nitric acid decomposition is rapid enough to be consistent with desorption followed by decomposition. Thus, if the zeolite acts as a collision partner, M, with an effect on the rate which is analogous to a pressure greater than 100 Torr, then $HNO_3(g)$ could be an intermediate.

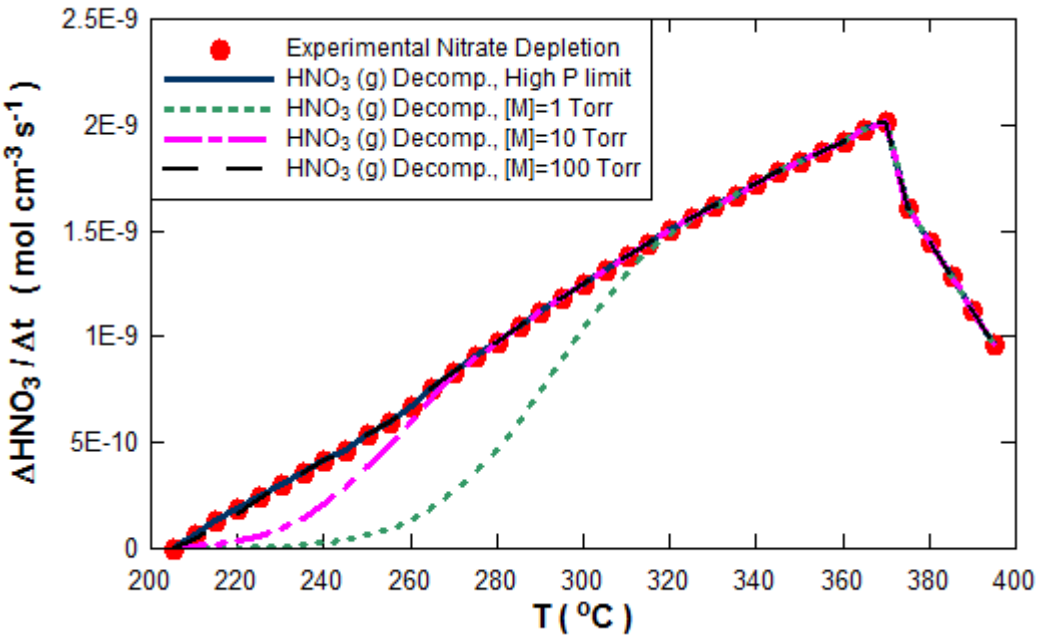

Figure S.2: Fitted experimental TPD curve for nitrate depletion with a comparison of the rate at which desorbing nitric acid would decompose for various pressures of M. For [M]=100 Torr and the high pressure limit, the curves overlap with the experimental nitrate depletion curve.

To find the pressure of M which the zeolite would have an effect comparable to, we calculate the gas phase pressure which has a mean free path comparable to that in the zeolite.[5] The internal pores of Faujasites, such as BaNa-Y, have average diameters between 7 to 10 Å.[6,7] The mean free path of a gas, λ, is approximated by[5]

$$\lambda = \frac{kT}{2^{1/2}\sigma\ p} \qquad \text{(S.5)}$$

where σ is the collision cross-section, p is the pressure, and k and T have their usual meanings. Taking generous limits of 100 Å^2 for σ of HNO_3 in Ar, and 20 Å for λ within the pores, over the temperature range of the TPD experiments (200 to 400 °C) the time between collisions in the zeolite pores then corresponds (by Eq. S.5) to a pressure of > 1 x 10^4 Torr .

The Lindemann rate constant can be found as a function of [M] by:[8]

$$k_{uni} = \frac{k_\infty}{1 + k_\infty /(k_0[M])} \qquad \text{(S.6)}$$

where k_∞ is the high pressure limit rate constant, and k_0 is the low pressure limit rate constant. Though deviations from the above expression occur with most real gases, using the above expression and the values of k_∞ and k_0 from Zhu and Lin with M = Ar,[9] shows that the high pressure limit is reached for HNO_3 at < 1 x 10^4 Torr (Figure S.3). We therefore expect the rate for HNO_3 decomposition in the pores to be dictated by the rate constant for the high pressure limit due to collisions with the zeolite pore walls, even though the maximum total pressure during experiments is ~50 Torr. As shown in Fig. S.2, this result indicates that $HNO_3(g)$ may be an intermediate during TPD.

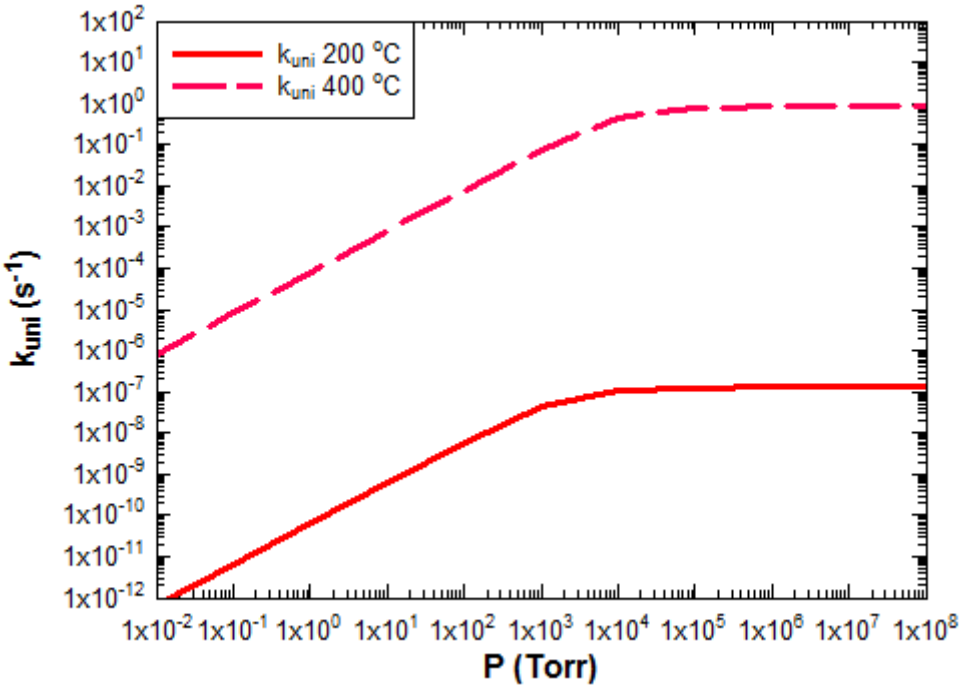

Figure S.3: The pseudo-first-order rate constant's pressure for the thermal decomposition of HNO_3(g) as a function of the pressure of M. The high pressure limit is reached at <10^4 Torr.

III. Steady State Approximation for [OH]

A steady state approximation can be used to set an upper limit for [OH]. From Section IV.B.1.b of the main article:

$$H^+ + NO_3^- \rightarrow HNO_3 \qquad \text{(S.7)}$$

$$HNO_3 \rightarrow OH + NO_2 \qquad (9)$$
$$OH + CO \rightarrow CO_2 + H \qquad (10)$$
$$HNO_3 \rightarrow OH + NO_2 \qquad (11)$$
$$H + OH + M \rightarrow H_2O + M \qquad (12)$$
$$2HNO_3 + CO \rightarrow 2NO_2 + CO_2 + H_2O \qquad (13)$$

Applying a steady state approximation on [OH]:

$$\frac{d[OH]}{dt} = k_9[HNO_3] - k_{10}[OH][CO] - k_{12}[H][OH][M] = 0 \qquad \text{(S.8)}$$

leads to

$$k_9[HNO_3] = k_{10}[OH][CO] + k_{12}[H][OH][M] \qquad \text{(S.9)}$$

The concentrations in this equation can be related to the experimental data. Since S.7 is rate limiting (see IV.A.1 of main article),

$$k_9[HNO_3] = -\frac{d[NO_3^-]}{dt} \qquad \text{(S.10)}$$

The consumption of OH in Eq. 10 is given by the experimentally observed production of CO_2. Thus,

$$k_{10}[CO][OH] = \frac{d[CO_2]}{dt} \qquad \text{(S.11)}$$

The mechanism in Eqs 9 to 12 requires that the OH consumed by Equation 12 is equal to that consumed by Equation 10. From stoichiometry,

$$k_{12}[H][OH][M] = k_{10}[CO][OH] = \frac{d[CO_2]}{dt} \qquad \text{(S.12)}$$

Substituting Eqs. S.10, S.11, and S.12 into Eq. S.9 gives,

$$-\frac{d[NO_3^-]}{dt} = 2\frac{d[CO_2]}{dt} \quad \text{(S.13)}$$

The derivatives can be approximated as changes, Δ, which are obtainable from the experimental data.

$$-\frac{\Delta[NO_3^-]}{\Delta t} = 2\frac{\Delta[CO_2]}{\Delta t} \quad \text{(S.16)}$$

The relationship shown in Eq. S.16 is accurate within experimental error over the experimental temperature range of 200-300 °C (Figure 5 of main paper reproduced below), indicating that the steady state approximation is valid for [OH].

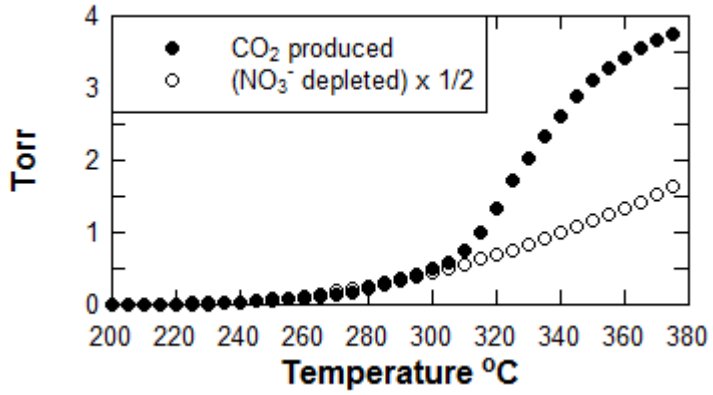

Figure 5: Production of CO_2 is half the nitrate depletion for temperatures < ~300 °C.

Given that the steady state approximation is valid for OH, the OH produced during any given time-step cannot exceed the nitrate depleted during that time-step. Based on the nitrate depletion during any given times-step, and using the scaling of moles of nitrate described in Section IV.A.2 of the main article, the maximum concentration of OH that is possible during a time-step of 1 second is $<10^{-2}$ Torr, assuming that the OH is homogeneously distributed within the reactor. As elaborated upon in Section B.1.b, the

reaction in Eq. 12 may actually occur within the zeolite with a local concentration greater than 10^{-2} Torr.

IV. Reaction of H+OH relative to H+H and OH +OH

In this section, we show that the values in Table S.2 (for Rxns 2-2b, 8-2, 8-8) suggest that the reaction of H + OH should dominate over the reactions of H + H and OH + OH if the zeolite pore walls act as a third body. This is true both in the low pressure limit, and in the high pressure limit, though, as justified below, we expect the high pressure limit to be operative in the zeolite.

Based on the mechanism in Eqns. 9 to 12, the quantity of H produced would equal the quantity of OH produced: [OH]=[H]. Given [OH]=[H], the relative magnitude of the rates constants of the second-order or pseudo-second-order rate constants determine the relative rates for Rxns 2-2b, 8-2, and 8-8. The total gas concentration during these experiments is $<10^{-5}$ mol cm^{-3}. Using the gas phase rate constants in the low pressure limit in Table S.2 (those which include "M" in the chemical equation), the rate constant for H+OH+M is ~$\geq$10 times greater than that for either H+H+M or OH+OH+M. Thus, the rate of reaction of H+OH would be greater by a factor ~$\geq$10 than that for either H+H or OH+OH even in the low pressure limit, but smaller than the rate of reaction of $H+NO_2$.

However, we anticipate that the zeolite acts as a third body. The collision cross-sections of H and OH are smaller than that of HNO_3, 7.40 $Å^2$ and 9.79 $Å^2$ respectively.[10] The analogous pressure for the zeolite acting as a collision partner is then still $>10^5$ torr from Eq. S.5. The equation describing the pressure dependence of the rate for radical combination reactions (i.e., A + B + M → AB + M) which is analogous to Eq. S.6

includes empirically obtained constants[11] that are not always available. However, the pressure at which the reaction rate approaches the high pressure limit (where an increase in the pressure of M does not lead to a further increase in the rate of the overall reaction) must be at a lower pressure than the pressure at which an intersection occurs between the extrapolation of the low pressure rate to higher pressures and the extrapolation of the high pressure rate to lower pressures. Thus, we can obtain an upper limit for the pressure at which the approach to the high pressure limit begins. Using the rate constants from the Table S.2, this intersection is shown for both the reaction of H+OH and the reaction of OH+OH in Figure S.4. As can be seen, in both cases the reaction rates approach the high pressure limit below 10^5 Torr. As mentioned, the zeolite would act as a collision partner analogous to a pressure of $>10^5$ Torr. This justifies the use of the high pressure limits as an approximation for the rates of these reactions; with the zeolite acting as a third body which effectively places the reaction rate into a regime analogous to what would be expected for a pressure of $[M] > 10^5$ Torr. For such a situation, the rate constant for the reaction of H + OH is >10 times larger than the rate constant for the reaction of OH + OH. To our knowledge the rate constant for the reaction of H+H is not available in,this high pressure regime. We assume that in the high pressure limit, the H+OH rate constant remains larger than that of the H+H reaction, much like with OH + OH. Thus, the H + OH reaction is expected to be dominant relative to the reaction of OH + OH and the reaction of H + H. As discussed in the main article, the H + OH reaction is also expected to dominate over the H + NO_2 reaction.

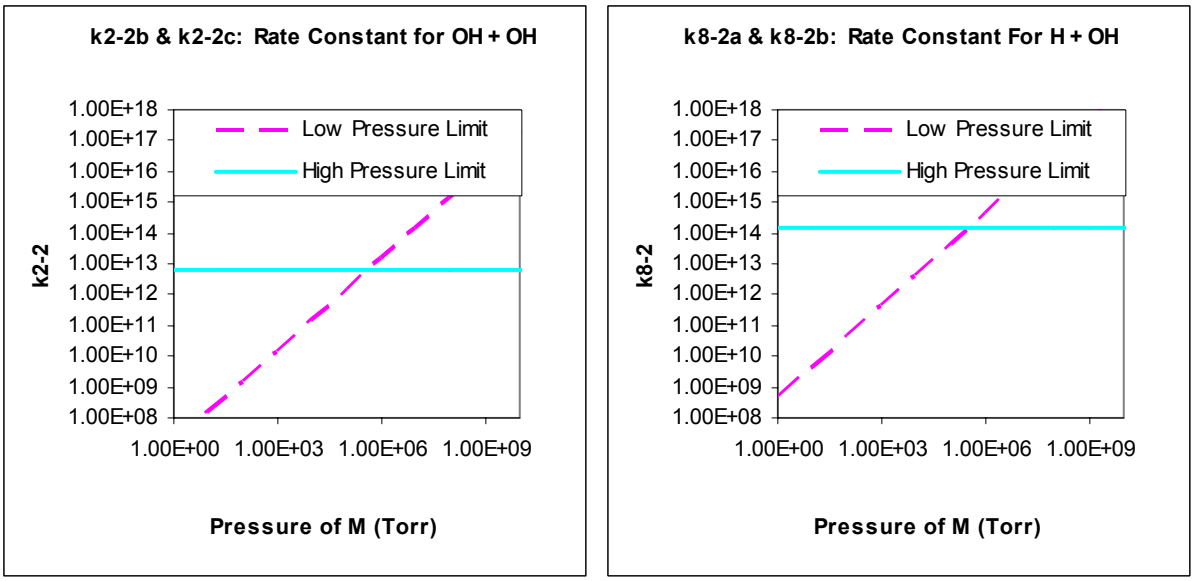

Figure S.4: Pseudo-second-order rate constants for H+OH and OH +OH reactions. The rate constant must begin approaching the high pressure limit prior to the intersections, and thus before 10^5 Torr. Units for pseudo-second-order rate constants (k) are $cm^3\ mol^{-1}\ s^{-1}$

V. Reaction of H+OH relative to OH + HNO_3

The data presented in this work demonstrate that in an evacuated zeolite environment the reaction of OH with H can dominate, whereas the reaction of OH + HNO_3 is normally the dominant consumer of OH when HNO_3 is heated in the gas phase.[12-14] However, increasing the pressure of HNO_3 in these experiments to a suitably high level should push the system into a regime where the reaction of OH + HNO_3 regains its dominance relative to the reaction of H+OH, based upon the accepted rate constants in Table S.2. In experiments performed at elevated temperatures (200 to 300 °C) with BaNa-Y, Na-Y, SiO_2, or only the tungsten grid and with excess HNO_3(g), the NO/NO_2 ratios obtained were consistent with the reaction of OH + HNO_3 being dominant relative to the reaction of OH + H.

VI. Evidence of WO_3 catalyzed Oxidation of CO above 300 °C

Subsequent to the TPD experiments described in the main article, the tungsten grids turned a light yellow color, indicative of WO_3. WO_3 (or WO_{3-x}) is a known catalyst for CO oxidation when oxygen is present.[15,16] Separate experiments conducted with a fresh tungsten grid exposed to only NO_2 at 300 °C showed that the tungsten grid is oxidized to WO_3 and WO_{3-x} by NO_2 (characterization described below). Subsequent addition of CO then showed that the oxidation of CO with NO_2 as the source of oxygen occurs by sequential steps with surface intermediates and/or surface modification. This was shown through the following set of experiments, conducted at both 300 °C and 400 °C:

1) Introduction of CO with a fresh grid at elevated temperatures showed no reaction.
2) Introduction of NO_2 followed by evacuation to remove all gaseous NO_2 and then introduction of CO showed oxidation of CO to CO_2.
3) Evacuation of the chamber followed by a repeat of 2) using the same tungsten grid still showed oxidation of CO to CO_2.

These experiments indicate that oxidation of CO, with NO_2 as the oxygen source, is catalyzed by the partially oxidized tungsten grid.

Characterization of the partially oxidized grids, which was conducted by x-ray powder diffraction, UV/vis Absorption, and IR Absorption, indicated that the grids were composed of W, WO_3, and non-stoichiometric WO_{3-x}. The UV/vis absorption qualitatively matched the spectra in the literature, with a strong adsorption in the 200 nm region which gradually decreased into the 400 nm region, giving rise to the yellow color

of WO_3.[17-19] The IR absorption spectrum showed broad overlapping infrared peaks from 800 to 1000 cm^{-1}, characteristic of W-O-W bridging and W=O stretching, indicative of WO_3 and WO_{3-x} respectively.[17,20,21] The x-ray powder diffraction pattern matched against diffraction pattern databases were also consistent with W, WO_3, and non-stoichiometric WO_{3-x} being present in the partially oxidized grids. These results are also consistent with literature reports that W is oxidized to WO_3 at these temperatures,[22] and that non-stoichiometric WO_{3-x} is formed during the oxidation of W to WO_3.[23]

Table S.1: Table of Reactants and Intermediates Considered‡

Chemical Formula		HNO_3	OH	NO_3	NO	NO_2	CO	CO_2	H	HONO	N_2O_4	H_2O	O	O_3	O_2	N_2O_3	HNO	HCO
	#	1	2	3	4	5	6	7	8	9	10	11	12	13	14	15	16	17
Nothing	0	√	x	x	x	x	x	x	x	√	√	x	x	√	x	√	√	
HNO_3	1	L?	√	x	x	x	x	x	L?	x?	L?	?	?	?	x	L?	L?	
OH	2		L	L	√	√	√	x	L	√	L?	?	L	L	√	L?	√	√
NO_3	3			L	√	√	√	x?	L	L?	L?	?	L	L	x	L?	L?	
NO	4				x	√	x?	x?	√	√	x	x?	√	√	√	L?	√	√
NO_2	5					√	√	x?	√	x	x	?	√	√	x	x?	√	√
CO	6						x	x	√	x	x	x?	√	x	x?	x?	√	
CO_2	7							x	√	x	x	x	√	x	x	x?	x?	
H	8								L	√	L?	?	L?	L	√	L?	L?	
HONO	9									L?	L?	?	√	L	x	L?	L?	
N_2O_4	10										L?	?	L?	L	x?	L?	L?	
H_2O	11											x	?	L?	x	?	?	
O	12												L	L	L?	L?	√	
O_3	13														x?	L?	L?	
O_2	14														x	L?	x?	
N_2O_3	15															L?	L?	
HNO	16																√	
HCO	17																	

Legend for initial assumptions:
√ assumed to be non-negligible
x assumed to be negligibly slow
L assumed negligible due to low concentrations
? uncertain contribution

‡Reactions for HO_2 (#18) not shown.

Table S.2. Rate Constant Parameters for Reactions Considered.
Units for Pre-exponentials: s^{-1} for 1st order, $cm^3\ mol^{-1}\ s^{-1}$ for 2nd order, $cm^6\ mol^{-2}\ s^{-1}$ for 3rd order.

Rxn #	Reaction	Pre-exponential	Activation Energy, Ea (J)	Order	Ref. †
1-0a	HNO_3 --> OH + NO_2 (+M, high pressure limit)	2.3E23T^-2.27	2.18E05	1st	9
1-0b	HNO_3 + M → OH + NO_2	1.58E15	1.34E05	2nd	24,25
1-2	HNO_3 + OH --> NO_2 + H_2O	6.20E09	-5.99E03	2nd	[a]
2-2a	OH + OH --> H_2O + O	1.51E9*T^1.4	0 or N/A	2nd	11
2-2b	OH + OH + M --> H_2O_2 + M	2.90E17*(T/300)^-7.6	0 or N/A	3rd	11
2-2c	OH + OH --> H_2O_2 (+M, high pressure limit)	9.03E12 *(T/300)^-0.37	0 or N/A	2nd	11
4-1	NO + HNO_3 --> NO_2 + HONO	Negligible. Only reported k's: k= 1E3 to 5E3 for 295-300K		2nd	[b]
4-2	NO + OH + M --> HONO + M	2.68E17*(T/300)^-2.4	0 or N/A	3rd	26
4-3	NO + NO_3 --> 2 NO_2	1.08E13	-914.54	2nd	26
5-0	NO_2 --> NO + O (+M, high pressure limit)	A_∞ = 7.6E18*T^-1.27	306645	1st	27
5-2a	OH + NO_2 + M-->HNO_3	1.20E42*T^-8.8	13792.9	3rd	9
5-2b	OH + NO_2 --> HO_2 + NO	1.81E13	27940	2nd	27,28
5-3	NO_2 + NO_3 + M --> N_2O_5 + M	1.30E18*(T/300)^-4.1	0 or N/A	3rd	26
5-3b	NO_2 + NO_3--> NO_2 + O_2 + NO	8.11E10	12690	2nd	[c]
5-4	NO + NO_2 + M --> N_2O_3 + M	2.57E14*(T/300)^-7.7	0 or N/A	3rd	26
5-4	NO_2 + NO +M --> N_2O_3 + M	1.12E14*(T/300)^-7.7	0 or N/A	2nd	26
5-5a	NO_2 + NO_2 +M --> N_2O_4	5.07E14(T/300)^-3.8	0 or N/A	3rd	26
5-5b	NO_2 + NO_2 --> 2NO + O_2	8.60E12	120499.2	2nd	29
5-5c	NO_2 + NO_2 --> NO_3 + NO	3.20E12	107528.8	2nd	29
6-2a	CO + OH --> CO_2 + H	6.32E6*T^1.5	-2078.5	2nd	11
6-3	CO + NO_3 --> CO_2 + NO_2	5.62E11	16160	2nd	30‡
6-5	CO + NO_2 --> CO_2 + NO	9.04E13	1.41E05	2nd	27
7-2	CO2 + OH --> CO + HO_2	Negligible, Ea > 250 kJ, and not included in [31]			32
7-4	NO + CO_2 --> NO_2 + CO	Negligible, k <3.01E9 at 3000K		2nd	[d]
8-2a	H + OH + M--> H_2O	8.3E21*T^-2.0	0 or N/A	3rd	11
8-2b	H + OH --> H_2O (+M, high pressure limit)	A_∞ = 1.62E14	620	2nd	33
8-4	H + NO + M --> HNO	3.46E19*T^-1.17	1762.568	3rd	27
8-5	H + NO_2 --> OH + NO	8.43E13	0 or N/A	2nd	27
8-6	CO + H + M --> HCO + M	6.3E20T^-1.82	15430.784	3rd	31
8-7	CO_2 + H --> CO + OH	1.51E14	110576.2	2nd	31
8-8	H + H + M --> H_2	6.5E17*T^-1.0	0 or N/A	3rd	11
9-0	HONO + M --> HO + NO + M	1.0E30*T^-3.59	209911.28	2nd	29
9-1	HONO + HNO3 -->	Assumed negligible, not included in [26,27,34]			26,27,34
9-2	HONO + OH --> H_2O + NO_2	3.76E12*T	565	2nd	27
9-4	*c*-HONO + NO --> NO_2 + HNO	1.5E11 (T/298)^2.64	1.69E04	2nd	[e]
9-5	NO_2 + HNO_2 --> HNO_3 + NO	Negligible. Slow at 25 °C,[35] and not included in [29]			35
9-6	HONO + CO_2	Assumed negligible, not included in [36]			36
9-7	HONO + CO	Assumed negligible, not included in [36]			36
9-8	HONO + H --> H_2 + NO_2	1.21E13	3.08E04	2nd	27
10-0a	N_2O_4 + M --> NO_2 + NO_2 + M	7.826E18(T/300)^-3.8	53209.6	2nd	26

12-4	$O + NO + M \rightarrow NO_2 + M$	5.22E15	-4.15E03	2nd	[26]
12-5a	$O + NO_2 \rightarrow NO + O_2$	3.27E12	-1.51E03	2nd	[f]
12-5b	$O + NO_2 + M \rightarrow NO_3 + M$	3.27E16*(T/298)^-2	0 or N/A	3rd	[37]
12-6	$CO + O + M \rightarrow CO_2$	6.16E14	12555.65	3rd	[31]
12-7	$CO_2 + O \rightarrow CO + O_2$	1.69E13	220321	2nd	[31]
12-9	$HONO + O \rightarrow OH + NO_2$	1.21E13	2.49E04	2nd	[27]
13-0	$O_3 + M \rightarrow O_2 + O + M$	4.31E14	9.31E04	2nd	[g]
13-5	$O_3 + NO_2 \rightarrow O_2 + NO_3$	8.43E10	20540	2nd	[26]
13-4	$O_3 + NO \rightarrow O_2 + NO_2$	8.43E11	10890	2nd	[26]
13-6	$CO + O_3 \rightarrow CO_2 + O_2$	negligible, k < 6E2 at 298		2nd	[h]
14-2	$OH + O_2 \rightarrow HO_2 + O$	2.23E13	220000	2nd	[31]
14-4a	$NO + NO + O_2 \rightarrow 2NO_2$	1.20E09	-4406.42	3rd	[26]
14-4b	$NO + O_2 + M \rightarrow NO_3$	2.05E07	1.75E03	3rd	[38]
14-8	$O_2 + H + M \rightarrow HO_2 + M$	2.25E16*(T/300)^-1.6	0 or N/A	3rd	[34]
14-12	$O_2 + O + M \rightarrow O_3 + M$	2.18E14*(T/298)^-2.80	0 or N/A	3rd	[37]
15-6	$N_2O_3 + M \rightarrow NO + NO_2 + M$	1.14E17*(T/300)^-8.7	40572.32	3rd	[26]
16-0	$HNO + M \rightarrow H + NO$	3.3E17*(T^-1.24)	2.10E05	2nd	[27]
16-2	$OH + HNO \rightarrow H_2O + NO$	1.73E12*(T/298)^1.07	1690	2nd	[i]
16-4	$HNO + NO \rightarrow OH + N_2O$	8.50E12	123789.50	2nd	[29]
16-5	$HNO + NO_2 \rightarrow NO + HONO$	1.80E12	29831.92	2nd	[29]
16-6	$CO + HNO \rightarrow CO_2 + NH$	2E12	51470	2nd	[j]
16-7	$HNO + CO_2 \rightarrow$	Assumed negligible, not included in [27]			[27]
16-12a	$HNO + O \rightarrow OH + NO$	3.61E13	0 or N/A	2nd	[27]
16-14	HNO + O2 --> products	2.2E10	318049	2nd	[k]
16-16a	$HNO + HNO \rightarrow H_2O + N_2O$	8.43E08	1.30E04	2nd	[27]
17-2	$HCO + OH \rightarrow H_2O + CO$	1.02E14	0 or N/A	2nd	[11]
17-4	$HCO + NO \rightarrow CO + HNO$	7.23E12	0 or N/A	2nd	[27]
17-5a	$HCO + NO_2 \rightarrow CO + HNO_2$	2.1*T^3.29	9810	2nd	[27]
17-5b	$HCO + NO_2 \rightarrow CO2 + NO + H$	1.17E14*T^-0.75	8070	2nd	[27]
18-2	$HO_2 + OH \rightarrow H_2O + O_2$	2.89E13	2080	2nd	[11,26]
18-4	$HO_2 + NO \rightarrow OH + NO_2$	2.17E12	2240	2nd	[26]
18-5	$HO_2 + NO_2 + M \rightarrow HO_2NO_2$	6.53E16*(T/300)^-3.20	0 or N/A	3rd	[26]
18-6	$HO_2 + CO \rightarrow CO_2 + OH$	1.51E14	98940	2nd	[31]
18-8a	$HO_2 + H \rightarrow H_2O + O$	3.01E13	7200	2nd	[11]
18-8b	$HO_2 + H \rightarrow OH + OH$	1.69E14	3660	2nd	[11]
18-8c	$HO_2 + H \rightarrow H_2 + O_2$	4.28E13	5900	2nd	[11]
18-12	$HO_2 + O \rightarrow OH + O_2$	3.25E13	0 or N/A	2nd	[11]
18-18	$HO_2 + HO_2 \rightarrow H_2O_2 + O_2$	1.87E12	6440	2nd	[11]
19-0	$HO_2NO_2 + M \rightarrow HO_2 + NO_2$	2.47E19	88130	2nd	[26]
19-2	$HO_2NO_2 + OH \rightarrow$ Products	1.14E12	-2.24E03	2nd	[26]

†References for values taken directly from http://kinetics.nist.gov are designated by letters in brackets and kept below in *squib* notation: the year of the citation, the first three letters of the last names of the first two authors, and the initial page number (and final page number if available) are utilized. If more than one reference is listed, then kinetics.nist.gov was used to fit the values from the references listed. Caution must be used with kinetics.nist.gov, as for non-Ahrennius forms the values provided often do not match those of the original reference.

‡ See Section IV.B.1.c, calculated using $k_{4\text{-}3}$.

[a]1990MAC/BAL1167, 1986STA/MOL2777, 1985CON/HOW17, 1984DEV/CAR94, 1982RAV/EIS1854, 1982MAR/WAT3819, 1982KUR/COR308, 1982JOU/POU5827, 1981WIN/RAV1105, 1999BRO/TAL3031-3037 [b]1979STR/WEL3439, 1979MCK/MAT779, 1977KAI/WU187, 1988SVE/LJU857 [c]1997DEM/SAN1-266, 1994DEM/SAN, 1992WAN/LJU7640-7645, 1989HJO/CAP5458, 1988CAN/DAV4997, 1975GRA236 , 1958SCH/DAV1841, 1951JOH4542-4546 [d]1969CLA/GAR2885 [e]1998MEB/LIN729-736 [f]2001EST/NIC9697-9703, 1999GIE/BUR877-883, 1997DEM/SAN1-266, 1987GEE/STU263, 1986ONG/BIR3359, 1973SLA/WOO615, 1974BEM/CLY564,

1991TSA/HER609-663 -- used only data with ranges instead of points. Result similar to but believed to be more accurate than [26] for these conditions. [g]1979HEI/COF117 [h]1973STE/NIK303, 1972ARI/WAR1514 [k]2004NGU/ZHA94-99, value similar to that of [27] [i]1994ROH/WAG975-981 [j]1993BRY/KAC392-398

References:

(1) Masel, R. I. *Principles of adsorption and reaction on solid surfaces*; Wiley: New York, 1996.

(2) Zhdanov, V. P.; Pavlicek, J.; Knor, Z. *Catalysis Reviews-Science and Engineering* **1988**, *30*, 501.

(3) Karge, H. G.; Dondur, V. *Journal of Physical Chemistry* **1990**, *94*, 765.

(4) Szanyi, J.; Kwak, J. H.; Peden, C. H. F. *Journal of Physical Chemistry B* **2004**, *108*, 3746.

(5) Atkins, P. W. *Physical chemistry*, Vers 6.0. ed.; Oxford University Press: Oxford, 1998.

(6) Chen, N. Y.; Degnan, T. F.; Smith, C. M. *Molecular transport and reaction in zeolites : design and application of shape selective catalysts*; Vch: New York N Y, 1994.

(7) Ohayon, D. Thermally Stable ZSM-5 Zeolite Materials With New Microporosities, Concordia University, 1998.

(8) Steinfeld, J. I.; Francisco, J. S.; Hase, W. L. *Chemical kinetics and dynamics*, 2nd ed.; Prentice Hall: Upper Saddle River N J, 1999.

(9) Zhu, R. S.; Lin, M. C. *Journal of Chemical Physics* **2003**, *119*, 10667.

(10) Halpern, A. M.; Glendening, E. D. *Theochem-Journal of Molecular Structure* **1996**, *365*, 9.

(11) Baulch, D. L.; Cobos, C. J.; Cox, R. A.; Esser, C.; Frank, P.; Just, T.; Kerr, J. A.; Pilling, M. J.; Troe, J.; Walker, R. W.; Warnatz, J. *Journal of Physical and Chemical Reference Data* **1992**, *21*, 411.

(12) Johnston, H. S.; Foering, L.; Tao, Y.-S.; Messerly, G. H. *Journal of the American Chemical Society* **1951**, *73*, 2319.

(13) Johnston, H. S.; Foering, L.; Thompson, R. J. *Journal of Physical Chemistry* **1953**, *57*, 390.

(14) Johnston, H. S.; Foering, L.; White, J. R. *Journal of the American Chemical Society* **1955**, *77*, 4208.

(15) Lin, H. M.; Tung, C. Y.; Hsu, C. M.; Lee, P. Y. *Journal of Materials Research* **1995**, *10*, 1115.

(16) Adams, K. M.; Gandhi, H. S. *Industrial & Engineering Chemistry Product Research and Development* **1983**, *22*, 207.

(17) Daniel, M. F.; Desbat, B.; Lassegues, J. C.; Garie, R. *Journal of Solid State Chemistry* **1988**, *73*, 127.

(18) Zayim, E. O.; Baydogan, N. D. *Solar Energy Materials and Solar Cells* **2006**, *90*, 402.

(19) Hutchins, M. G.; Abu-Alkhair, O.; El-Nahass, M. M.; El-Hady, K. A. *Materials Chemistry and Physics* **2006**, *98*, 401.

(20) Antonaia, A.; Santoro, M. C.; Fameli, G.; Polichetti, T. *Thin Solid Films* **2003**, *426*, 281.

(21) Orel, B.; Groselj, N.; Krasovec, U. O.; Jese, R.; Georg, A. *Journal of Sol-Gel Science and Technology* **2002**, *24*, 5.

(22) Warren, A.; Nylund, A.; Olefjord, I. *International Journal of Refractory Metals & Hard Materials* **1996**, *14*, 345.

(23) Sikka, V. K.; Rosa, C. J. *Corrosion Science* **1980**, *20*, 1201.

(24) Baulch, D. C.; Drysdale, D. D.; Horne, D. G. Homogeneous Gas Phase Reactions of H2-N2-O2 System. In *Evaluated Kinetic Data for High Temperature Reactions, Vol. 2*; Butterworth: London-New York, 1974; pp 421.

(25) Ballod, A. P.; Titarchuk, T. A.; Tiker, G. S.; Rozovskii, A. Y. *Kinetics and Catalysis* **1989**, *30*, 677.

(26) Atkinson, R.; Baulch, D. L.; Cox, R. A.; Crowley, J. N.; Hampson, R. F.; Hynes, R. G.; Jenkin, M. E.; Rossi, M. J.; Troe, J. *Atmospheric Chemistry and Physics* **2004**, *4*, 1461.

(27) Tsang, W.; Herron, J. T. *Journal of Physical and Chemical Reference Data* **1991**, *20*, 609.

(28) Allen, M. T.; Yetter, R. A.; Dryer, F. L. *International Journal of Chemical Kinetics* **1995**, *27*, 883.

(29) Thaxton, A. G.; Hsu, C. C.; Lin, M. C. *International Journal of Chemical Kinetics* **1997**, *29*, 245.

(30) Brown, F. B.; Crist, R. H. *Journal of Chemical Physics* **1941**, *9*, 840.

(31) Tsang, W.; Hampson, R. F. *Journal of Physical and Chemical Reference Data* **1986**, *15*, 1087.

(32) Allen, T. L.; Fink, W. H.; Volman, D. H. *Journal of Physical Chemistry* **1996**, *100*, 5299.

(33) Cobos, C. J.; Troe, J. *Journal of Chemical Physics* **1985**, *83*, 1010.

(34) Atkinson, R.; Baulch, D. L.; Cox, R. A.; Hampson, R. F.; Kerr, J. A.; Troe, J. *Atmospheric Environment Part a-General Topics* **1992**, *26*, 1187.

(35) England, C.; Corcoran, W. H. *Industrial & Engineering Chemistry Fundamentals* **1974**, *13*, 373.

(36) He, Y. S.; Kolby, E.; Shumaker, P.; Lin, M. C. *International Journal of Chemical Kinetics* **1989**, *21*, 1015.

(37) Atkinson, R.; Baulch, D. L.; Cox, R. A.; Hampson, R. F.; Kerr, J. A.; Rossi, M. J.; Troe, J. *Journal of Physical and Chemical Reference Data* **1997**, *26*, 1329.

(38) Ashmore, P. G.; Burnett, M. G. *Transactions of the Faraday Society* **1962**, *58*, 253.